# Modeling steady-state dynamics of macromolecules in exponential-stretching flow using multiscale molecular-dynamics–multiparticle-collision simulations

Dhairyasheel Ghatage[1] and Apratim Chatterji[2,*]

[1]*Mechanical Engineering Department, College of Engineering, Shivajinagar, Pune-411005, India*

[2]*IISER-Pune, 900 NCL Innovation Park, Dr. Homi Bhaba Road, Pune-411008, India*

(Received 3 June 2013; published 10 October 2013)

We introduce a method to obtain steady-state uniaxial exponential-stretching flow of a fluid (akin to extensional flow) in the incompressible limit, which enables us to study the response of suspended macromolecules to the flow by computer simulations. The flow field in this flow is defined by $v_x = \epsilon x$, where $v_x$ is the velocity of the fluid and $\epsilon$ is the stretch flow gradient. To eliminate the effect of confining boundaries, we produce the flow in a channel of uniform square cross section with periodic boundary conditions in directions perpendicular to the flow, but simultaneously maintain uniform density of fluid along the length of the tube. In experiments a perfect elongational flow is obtained only along the axis of symmetry in a four-roll geometry or a filament-stretching rheometer. We can reproduce flow conditions very similar to extensional flow near the axis of symmetry by exponential-stretching flow; we do this by adding the right amounts of fluid along the length of the flow in our simulations. The fluid particles added along the length of the tube are the same fluid particles which exit the channel due to the flow; thus mass conservation is maintained in our model by default. We also suggest a scheme for possible realization of exponential-stretching flow in experiments. To establish our method as a useful tool to study various soft matter systems in extensional flow, we embed (i) spherical colloids with excluded volume interactions (modeled by the Weeks-Chandler potential) as well as (ii) a bead-spring model of star polymers in the fluid to study their responses to the exponential-stretched flow and show that the responses of macromolecules in the two flows are very similar. We demonstrate that the variation of number density of the suspended colloids along the direction of flow is in tune with our expectations. We also conclude from our study of the deformation of star polymers with different numbers of arms $f$ that the critical flow gradient $\epsilon_c$ at which the star undergoes the coil-to-stretch transition is independent of $f$ for $f = 2$, 5, 10, and 20.

DOI: 10.1103/PhysRevE.88.043303 PACS number(s): 02.70.−c, 47.57.Ng, 47.61.−k, 47.50.−d

## I. INTRODUCTION

The two most commonly occurring flows of complex fluids in nature are shear flow and extensional flow or a combination of the two. However, the response of soft matter to shear flowhas been much more investigated than extensional flow. In shear flow the velocity gradient is perpendicular to the flow velocity, i.e., the shear rate $\epsilon_s = dv_x/dy$; whereas in elongational flow the gradient in velocity is in the same direction as the flow, i.e., $\epsilon = dv_x/dx$. We have supposed that the fluid flows in the $x$ direction. One of the reasons for this greater focus on shear flow is the difficulty in obtaining elongational flow under controlled experimental conditions, as well as the difficulties involved in modeling it in simulations.

Before the advent of the filament-stretching rheometer [1–5], doing controlled extensional (or elongational flow) (henceforth referred to as E flow) experiments on viscoelastic materials was fraught with artifacts, and thereby different methods gave very different values of the extensional viscosity $\eta_E$. This was because of the transient nature of the flow obtained in each method, each with different induced flow histories. Furthermore, in some cases measurements were done before the steady-state condition was fully realized. In the celebrated M1 experiments [6–8] the $\eta_E$ of the same polymeric fluid code named M1 (0.244% polyisobutylene in a mixed solvent consisting of 7% kerosene in polybutene with molecular weight of $3.8 \times 10^6$) was measured by a wide variety of extensional rheometers and the values of $\eta_E$ obtained differed by over three orders of magnitude. This of course pointed to the need of developing better and standardized techniques to measure the $\eta_E$ of a complex fluid. Theoretical studies have also made limited progress as a result: a number of constitutive equations to quantify stress–strain-rate relationships under E flow exist, but different responses obtained in different flow measurement apparatuses led to a lack of proper validation of the constitutive relations [9].

Multiscale simulation of uniaxial planar elongational flow (refer to [10] for definitions of different kinds of elongational flow) can fill in the missing links between constitutive equations and experiments and provide a mesoscopic picture of the response of macromolecules to elongational flow; such techniques can also be used to calculate bulk stress with varying strain rate. But difficulties exist in modeling *steady-state* elongational flows in simulations with suitable boundary conditions such that bulk flow conditions are reproduced. A solution was proposed by Kraynik and Reinelt [11] which enabled suitable averaging of thermodynamic quantities in E flows. Previous simulation studies by various groups have focused on calculating a range of properties of polymeric systems in elongational flow. These include calculation of the elongational viscosity $\eta_E$ as a function of strain rate $\epsilon$ for dense alkanes and other bead-spring models of polymers [12–19], studies on the distribution of coil-stretch transition times for single polymer chains as a function of $\epsilon$ [20–28], calculation of diffusion constants of polymeric molecules

*apratim@iiserpune.ac.in

 

in flow [29,30], as well as study of the effect of solvent quality on the coil-stretch transition in flow [31]. All these studies used one of the two available technique for their simulations: (a) nonequilibrium molecular dynamics (NEMD) using Kraynik-Reinelt (KR) boundary conditions [11] or (b) Brownian dynamics (BD) simulations. NEMD methods using KR boundary conditions do not produce uniaxial or biaxial flows in steady state [15–18,29,30], although NEMD can be used to achieve transient uniaxial flows [12–14]. Moreover, the effects of hydrodynamic interactions between particles are not incorporated in the method, so it is unsuitable for studying the response of dilute systems in elongational flow. Hydrodynamic interactions are included in Brownian dynamics simulations [22–26,31–33], but the friction constant $\zeta$ of polymers is a parameter of the simulation and thus the change in $\zeta$ due to deformation in flow has to be calculated separately and included in the BD simulation.

In the last decade multiparticle-collision (MPC) dynamics has been extensively used to incorporate hydrodynamic interactions in studying the dynamics of soft matter systems in equilibrium as well as in flow [34–46]. The MPC fluid, just like the Lattice-Boltzmann simulation technqiue [47], is a coarse-grained model of the fluid which reproduces very well the fluctuating hydrodynamics of nearly incompressible fluids in flows with low Reynolds number and low Mach number.

In this work, we use the MPC simulation scheme to achieve steady-state exponential-stretching flow (ES flow) in a box of uniform cross section with periodic boundary conditions in all directions. ES flow is akin to E flow, and we show in this paper that polymers in ES flow get stretched above a critical flow gradient just as in E flow. In elongational flow the velocity of the fluid increases linearly in the flow direction (say $x$), $v_{fl} = \epsilon x$; furthermore, mass conservation demands $v^y_{fl} = -\epsilon y$. However, for ES flow, we maintain the most important characteristic for E flow, viz., $v_{fl} = \epsilon x$, but uniform fluid density along the length of a channel of uniform cross section is maintained by addition of suitable amounts of fluid from transverse directions. The typical soft matter constituents, colloid, polymer, or ampiphilic molecules, are embedded in the fluid and flow along the fluid with the imposed velocity gradient of ES flow. To maintain incompressibility of the background fluid with increasing velocity in the flow direction but with fixed number of particles within the simulation box, the continuity equation demands a box with tapering walls along $x$; however, a box of uniform cross section is desirable to avoid unwanted artifacts due to variable confinement with tapering walls.

However, if (1) a *fixed amount* of fluid of volume $dv$, (2) in a channel of uniform cross section, (3) were to have a velocity field $v_x = \epsilon x + v_0$, then the density of the fluid necessarily would have to decrease along the length of the channel. That we consider undesirable. What we show, however, is that if fluid is added along the length of the channel at an appropriate constant rate independent of $x$, then (1) the density can be maintained uniform along the length of the channel and (2) simultaneously maintain the desired velocity field.

Moreover, to maintain steady-state conditions with continuous flow in the simulation box with periodic boundary conditions (PBC), we would have to deal with a discontinous jump in velocity as well as the excess of fluid particles exiting the box with finite velocity at the $x = L_x$ end compared to the $x = 0$ end, i.e., the point where the fluid reenters the simulation box due to the PBCs. We tackle both the issues by (a) addition of fluid along the length of the channel, and (b) velocity discontinuity at the end of the simulation box with one ingenious idea to obtain a linearly increasing fluid velocity profile of a fluid of fixed density $\rho_{fl}$, but also in a box of uniform cross section. We just recycle the excess fluid coming out of the $x = L_x$ end and redistribute the same fluid along the length of the box to maintain constant $\rho_{fl}$.

The rest of the paper is organized as follows:

(a) In Sec. II we first give a brief overview of the MPC method, then we present our model to obtain steady-state uniaxial ES flow of the MPC fluid and finally demonstrate the success of our idea by our simulation results.

(b) In Sec. III, we describe our model and simulation results for two test cases where we embed macromolecules in our MPC fluid undergoing ES flow and study their response to the flow. We consider a colloidal suspension with just excluded volume interactions as the first test system, and star polymers with different arm numbers in E flow as the second test case.

(c) Finally we conclude in Sec. IV and discuss future prospects of extensions of this study to study various soft matter systems in ES flow.

## II. EXPONENTIAL-STRETCHING FLOW OF A MPC FLUID

### A. Model

We consider a volume of fluid undergoing ES flow in the $x$ direction. In our simulations, the fluid flows through a channel of length $L_x a$ and with square cross section of dimensions $L_y a \times L_z a$, where $a = 1$ is the unit of length in our system. We shall set the size of the cubic collision boxes of the MPC fluid to be $a$ (see later). We apply periodic boundary conditions in the $z$ and $y$ directions to model the bulk flow of fluid and avoid the effect of confining walls. For exponential-stretching flow of fluid, the velocity of fluid $v_x$ in the $x$ direction increases linearly with $x$:

$$v_x = \epsilon x + v_0. \tag{1}$$

The fluid enters the simulation box with velocity $v_0$ (=0 in our simulations) at $x = 0$ and the ES strain rate is $\epsilon$. This immediately implies that there is a force

$$\begin{aligned} f^x_{ES} &= m\frac{dv_x}{dt} = m\frac{\partial v_x}{\partial t} + mv_x\frac{\partial v_x}{\partial x} \\ &= mv_x\epsilon = m(\epsilon^2 x + \epsilon v_0) \end{aligned} \tag{2}$$

acting on each element of the fluid with mass $m$. The term $m\frac{\partial v_x}{\partial t} = 0$ in steady-state conditions. The displacement $X$ of the fluid element along the $x$ direction as a function of time is similarly obtained as

$$X = \frac{v_0}{\epsilon}(e^t - 1), \tag{3}$$

where the integration constant is obtained by defining $x = 0$ at time $t = 0$.

Since we aim to study the response of complex fluid systems in steady-state exponential-stretching flows, our simulation scheme has to address the two modeling issues mentioned

above: how to (A) maintain an ES flow of fluid in a simulation box of dimensions $L_x \times L_y \times L_z$ while maintaining a uniform fluid density $\rho_{fl}$ throughout, and (B) obtain a scheme to implement periodic boundary conditions for the background fluid in the $x$ direction, since there will be velocity discontinuity at $x = L_x$ for the fluid, as well as for the colloids or polymers or any other macromolecule one wishes to study in steady-state ES flow.

We use MPC dynamics to model the volume of fluid undergoing ES flow; the MPC fluid consists of $N_{fl}$ discrete noninteracting point particles of mass $m$ contained in a box of volume $V = L_x \times L_y \times L_z a^3$. MPC dynamics is a coarse-grained particle-based model of a fluid; it has become one of the established methods to model and incorporate hydrodynamic interactions between molecules of soft matter systems. There are many articles on the MPC method; it is also referred to as stochastic rotation dynamics in the literature [38,39]. Here we summarize the basic principles which MPC dynamics uses to model an equilibrium fluid, before we go on to describe a MPC fluid in ES flow. The interested reader can refer to the many other previous papers and review articles for the details of the method [34,36,37,40].

MPC dynamics consists of two steps, the ballistic motion step (position update step) and the collision step (velocity update step). In the ballistic step the MPC particles move in a straight line for time $h$ with their respective velocities $\vec{v}_i$ $(i = 1,2,\ldots,N_{fl})$ like particles of an ideal gas. However, the difference from a real gas is that all the $N_{fl}$ MPC particles move ballistically for an identical period of time $h$, before undergoing collisions. Thus, all $N_{fl}$ particles undergo collisions at the same instant of time after every time step $h$.

In the collision step, instead of having two-body collisions between particles with just two particles colliding and exchanging momentum, clusters of MPC particles undergo collision and redistribute momenta among themselves. Clusters of particles are identified by sorting all the particles into small cubic boxes of volume $a^3$, and the particles within a particular box exchange momenta in a collision. The linear dimension of the collision boxes $a$ is taken to be the unit of length for our system. To achieve redistribution of momentum, one first selects the inertial frame in which the total momentum of a selected cluster of $n_b$ particles belonging to a particular collision box is zero. That is, the velocities $\vec{v}'$ of MPC particles in this new frame are $\vec{v}'_n = \vec{v}_n - \vec{v}_{c.m.}$ such that $m\sum_n \vec{v}'_n = 0$, where $\vec{v}_{c.m.}$ is the center-of-mass velocity of $n_b$ particles, and the index $n = 1,2,\ldots,n_b$. Next, in this frame one rotates the velocity of each of the $n_b$ particles about a *random direction* by a *fixed angle* $\alpha$. This step redistributes momenta among the particles, maintaining energy and momentum conservation. One then adds back $\vec{v}_{c.m.}$ to the velocity of all the particles to get the new velocity of each of the $n_b$ particles in the original frame. This is repeated for all the collision boxes. One thus obtains momentum redistribution among $n_b$ particles due to collisions at one instant of time but simultaneously achieving local energy-momentum conservation throughout the system. To maintain Galilean invariance, one also has to do a random shift of collision boxes before the collision step; refer to [40] for details. Angular-momentum conservation is not maintained in this collision step, but there exists also an angular-momentum-conserving MPC method [40,41].

Variation of the values of the important parameters, viz., the density $\rho_{fl}$ of the fluid, the time between collisions $h$, and the rotation angle $\alpha$, can lead to a model of the fluid with a wide range of viscosity $\eta_f$ and Schmidt numbers Sc, which can be tuned *a priori*. The Schmidt number (Sc) is the ratio of momentum diffusivity and mass diffusivity; the dynamics of particles with high Sc is more liquidlike with momentum transport occurring predominantly via collisions, whereas a fluid with low values of Sc is more gaslike with momentum transfer occurring mainly by diffusion and mass motion of the constituent particles. For small values of $h$ and large values of $\alpha$, most of the momentum transport by the fluid is by collisions, akin to that of a liquid at a temperature $k_BT$.

*Units*. Energy values in our simulations are measured in units of the room temperature $k_BT$, and we set $k_BT = 1$. The unit of mass is the mass $m_f$ of a MPC fluid particle, and thereby the unit of time $\tau$ is fixed automatically by $k_BT/(m_f a^2) = 1/\tau^2$. At room temperature (300 K), with $a = 0.1$ $\mu$m and $m = 10^6$ a.u., $\tau \approx 10^{-7}$ s.

If now an externally applied force field of $f_E^x$ [see Eq. (2)] is applied to each MPC fluid particle of mass $m$, one can expect to obtain a velocity profile of $v_x = \epsilon x + v_0$ of the fluid. In the expression it is implicitly assumed that the fluid enters the channel at $x = 0$ with average velocity $(v_0,0,0)$ and we set $v_0 = 0$ for most of our simulations. However, a gradually increasing fluid velocity along the length of the channel would result in the decrease of the fluid density $\rho_{fl}(x)$ along $x$. This problem, identified as issue (A) before, would render this method useless to study complex fluids suspended in an incompressible fluid undergoing ES flow. Implementation of PBCs, issue (B), is a problem also because for an incompressible fluid the number of fluid particles $N_l$ crossing the $x = 0$ plane with the $x$ components of their velocities in the $-\hat{x}$ direction is always less than the number of particles $N_r$ moving right and crossing the $x = L_x$ plane with the $x$ components of their velocities in the $+\hat{x}$ direction. Refer to Fig. 1 for a schematic diagram. This is because the $N_r$

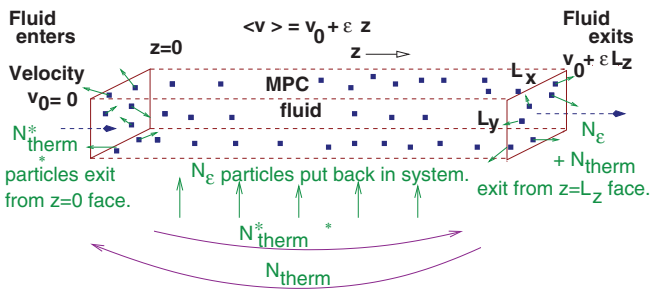


FIG. 1. (Color online) Schematic diagram to illustrate how we implement exponential-stretching flow, with velocity linearly increasing in the positive $x$ direction and a velocity discontinuity at $x = L_x$. $N_r = N_{\text{thermal}} + \langle N_\epsilon \rangle$ particles exit the $x = L_x$ plane to the right, whereas $N_l = N^*_{\text{therm}}$ exit at $x = 0$ to the left. $N_{\text{thermal}}$ and $N_l$ particles are put back into the left edge and right edge of the box using normal PBCs but with a suitable velocity shift by $\epsilon L_x$. $N_\epsilon$ particles are put at randomly chosen $x$ positions in the box with its $y,z$ coordinates remaining unchanged but with suitable shift in the $x$ velocity. Normal PBCs have been implemented for particles leaving the simulation channel in the $\pm\hat{y}$ and $\pm\hat{z}$ directions.

particles will have velocity contributions due to the ES flow which is over and above the thermal velocities. Thus, due to the higher $x$ velocity of particles near $x = L_x$, $\langle N_r \rangle$ will always be greater than $\langle N_l \rangle$ for a fluid with uniform density along $x$.

We use one idea as a solution to both the issues: the *excess* particles coming out of the right-hand side (RHS) of the box at $x = L_x$ are distributed in such a way that a uniform density of fluid particles is maintained throughout the box. A simple calculation shows that the excess particles $\langle N_\epsilon \rangle = \langle N_r \rangle - \langle N_l \rangle$ exiting the $x = L_x$ plane in each step must be distributed uniformly along $x$ to maintain $\rho_{fl}$ independent of $x$. This can be deduced by observing that in the steady state $\vec{\nabla} \cdot (\rho_{fl} \vec{v}) = \rho_{fl} \vec{\nabla} \cdot \vec{v} = \rho_{fl} \epsilon$, i.e., independent of $x$ in ES flow if one maintains $\rho_f = \text{const}$. Then the rate of addition of particles in a unit volume should also be $\rho_{fl}\epsilon$ and independent of $x$. These ideas are presented schematically in Fig. 1. Usually the expression $\vec{\nabla} \cdot \vec{v}_{fl} = 0$ holds true to express incompressibility conditions such that uniform density prevails for a fixed amount of fluid; however, note that we have $\vec{\nabla} \cdot \vec{v}_{fl} \neq 0$. Of course, in our case we have to add fluid particles locally to maintain $\rho_{fl} = \rho_0$ and simultaneously have the desired flow field in a box of uniform cross section. Globally there is mass conservation, i.e., the total number of fluid particles in the simulation box is strictly conserved as the number of excess particles exiting the box at the right are added back into the box along its length. But locally, mass is not conserved in our system.

The next question to address is the calculation of the value of $\langle N_\epsilon \rangle$ exiting the RHS of the simulation box in unit time due to ES flow. The net number of particles exiting the $x = L_x$ plane is $\vec{J}_f \cdot \vec{A} = (\rho_{fl} \epsilon L_x)(L_y L_z)$ per unit time, where $\vec{J}_f$ and $\vec{A}$ is the particle current density due to the flow and cross-sectional area of the tube, respectively. Therefore, in time $h$, i.e., one MPC update, the number of particles exiting the $x = L_x$ surface is $\langle N_\epsilon \rangle = \rho_{fl}(\epsilon L_x) L_y L_z h$: these are distributed with uniform probability along the length of the box. Thus the implementation of PBCs for the fluid particles can be summarized as follows: Suppose at a certain instant in time, $N_l$ and $N_r$ fluid particles cross the $x = 0 = L_x$ plane from right to left and left to right, respectively, at the end of a ballistic step. Then:

(a) All the $N_l$ particles are put back in the box at the RHS of the box as per standard molecular-dynamics PBC rules but with a velocity increment of $\epsilon L_x$ for the $x$ component of the velocity $v_x$ of all these particles. The $y$ and $z$ positions as well as the $v_y$ and $v_z$ of the $N_l$ particles remain unchanged.

(b) $N_{\text{thermal}} = N_r - \langle N_\epsilon \rangle$ number of particles are put back at the LHS (left-hand side) of the box, but with $v_x$ of these particles changed by an amount $-\epsilon L_x$; the $y,z$ coordinates and $v_y, v_z$ velocities remain unchanged.

(c) A random position $x_R$, where $0 \leqslant x_R \leqslant L_x$, is chosen for $\langle N_\epsilon \rangle$ particles using a uniform random number generator and the particles are put in this new position with the velocity suitably reduced by $(L_x - x)\epsilon$. The $y$ and $z$ positions and velocities remain unchanged.

Thus all the particles $N_r + N_l$ which exit the simulation box at the end of the position update step of the MPC scheme are retained in the box; this ensures particle number and correspondingly mass conservation at all times. The numbers

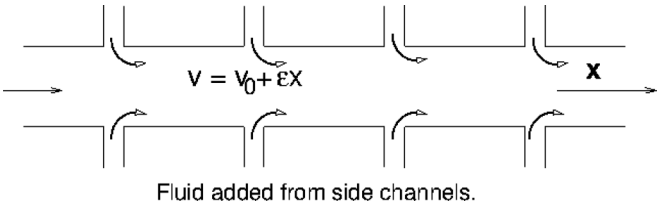


FIG. 2. A schematic diagram of a plausible experimental realization of a flow which will be similar (but not identical) to the flow in our simulation model with input of fluid along the entire length of the box (refer to Fig. 1). Introduction of particles at a constant rate at random positions independent of $x$ in the box is equivalent to a constant influx of fluid through side channels in a tube with the appropriately adjusted velocity $v_x$. Mass conservation is maintained: the amount of incoming fluid should be equal to the amount of fluid leaving the tube due to ES flow.

$N_l$ and $N_r$ are fluctuating quantities and $N_r > N_l$ always, but after a fixed number $N_\epsilon$ of the $N_r$ particles are redistributed in the box at random positions, the remaining $\langle N_r - \langle N_\epsilon \rangle \rangle$ is equal to $\langle N_l \rangle$. The introduction of particles at random positions along the length of the box might appear contrived; however, a situation demonstrating the underlying principle of introduction of particles along the length of the box can be plausibly experimentally realized as shown in Fig. 2.

The introduction of particles at random positions in the box is akin to pumping in fluid through side channels of the tube to maintain uniform density of the fluid undergoing ES flow. While the practicability of the idea can be answered only by doing an actual experiment, we envisage it as if there are an infinite number of tiny pores through which the right amounts of fluid are introduced back into the system. One can think of tiny amounts of fluid leaking back into the channel from the surface, with the appropriate local $x$ velocity of the fluid. Of course experimentally there can be only finitely many number of pores along the walls of the channel and there would always be a finite $y$ component of velocity for the fluid entering the channel. This would render the experimental realization close but never identical to our model of flow, where the thermally averaged fluid velocity has a component only in the $+\hat{x}$ direction. But then one can observe the flow and measure the response of soft matter systems more in the center of the experimental channel along the axis. We emphasize, however, that we also maintain PBCs in the $y$ and $z$ directions as we would like to investigate bulk ES flow of fluid.

To maintain incompressibility conditions in the fluid flow of any coarse-grained simulation method, one should ensure that the simulated fluid velocities are significantly less than the sound velocity of the model fluid (Mach number $\text{Ma} \ll 1$). To that end we have been careful to maintain the maximum value of the fluid velocity at values significantly less than the sound velocity $c_s$ [$c_s^2 = \gamma k_B T/m = 1.4(a/\tau)^2$, where $\gamma$ is the adiabatic index] of the fluid; in our case the fluid velocity near the $x = L_x$ end is the maximum fluid velocity $v_x^{\max}$ obtained in our simulations. For our simulations $v_x^{\max}$ is always $\leqslant 0.05 c_s$ unless otherwise mentioned. An appropriate MPC thermostat [48] is applied to maintain the temperature at a constant fixed value, otherwise the average kinetic energy of the system will gradually increase due to the externally applied $f_{ES}^x$ which sustains ES flow. We set the unit of length $a = 1$, unit of

energy $k_BT = 1$, unit of mass the mass of the fluid particle $m_f = 1$, and thereby the unit of time is $\tau = \sqrt{m_f a^2/k_BT}$. Then we choose the collision time $h = 0.1\tau$, $\rho_f = 10$, $\alpha = 130^\circ$ in a box of $L_x = L_y = L_z = 20a$ or $40a$ to test our model of steady-state ES flow of the background fluid.

### B. Results

Figure 3 shows the parallel streamlines in ES flow of a MPC fluid in a box of uniform cross section, where each fluid particle is acted upon by a force as explained in Eq. (2) with $\epsilon = 0.004a/\tau$ in a box of $(20a)^3$. The figure shows that the velocity near $x = 0$ is nearly zero and it goes on increasing with increasing value of $x$ and is maximum at $x = L_x$. Although the simulation box size is $(20a)^3$, the plotted box extends to $21a$ in the $x$ direction to accommodate the length of the arrow. The streamlines clearly indicate that the flow is pure uniaxial flow of fluid with increasing velocity only in the $x$ direction, reminiscent of E flow, but no velocity components in the transverse directions as one would expect in elongational flow. We maintain the appropriate velocity gradient in the direction of flow (in this case the $\hat{x}$ direction) by a suitable position-dependent force; in experiments with elongational flow, this is realized by the appropriately moving boundaries.

The streamlines for ES flows that we produce in our simulations might seem counterintuitive to most researchers, as the textbook definition [10] of the velocity fields for E flow is given not only as $v_x = ex$ but also $v_y = -ey$; this additional flow in the $y$ direction is dictated by the condition of mass conservation of an incompressible fluid. In our simulations, however, mass conservation is inherent in our model as only

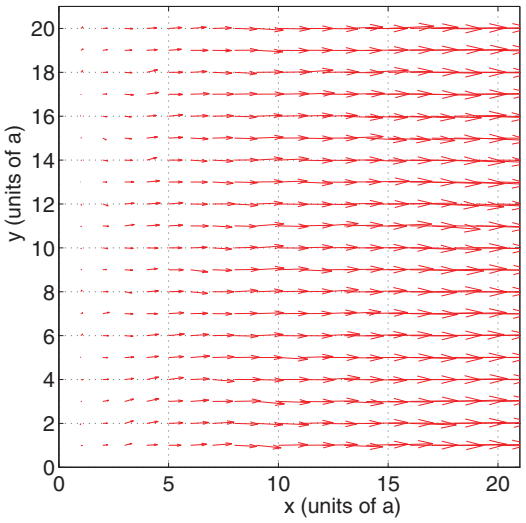


FIG. 3. (Color online) Streamlines of a MPC fluid in ES flow with $v_x^{\max} = \epsilon L_x = 0.08a/\tau$ in a box of volume $(20a)^3$ with $\epsilon = 0.004\tau^{-1}$. The fluid velocity increases linearly with $x$. Since there is a slow but gradual flux of fluid into the simulation box along the sides of the channel (refer to Fig. 2) at the same rate at which the fluid gets drained out of the channel, we do not obtain the typical streamlines observed in elongational flow experiments with $v_x = \epsilon x$ and $v_y = -\epsilon y$. The streamlines observed in our simulations are close to what might be expected at the central axis of a complex fluid flow in a filament-stretching rheometer.

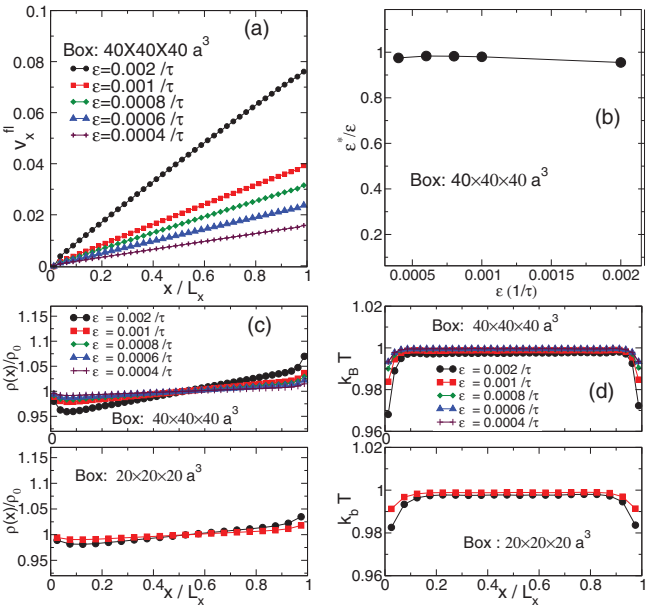


FIG. 4. (Color online) (a) Plot of the fluid velocity $v_x^{fl}$ of a MPC fluid along the flow direction $x$. $v_x^{fl}$ increases linearly along $x$. The quantity $x$, the distance from the point where the fluid enters the box, has been normalized by box length $L_x$. (b) Ratio of the velocity gradient $\epsilon^*$, the slope calculated from velocity profile in (a), and the applied flow gradient $\epsilon$ versus $\epsilon$. (c) Plot of the number density profile $\rho(x)$ of the MPC particles versus $x$, which remains uniform along $x$. The quantity $\rho(x)$ is normalized by the average number density $\rho_0$ of the fluid. (d) The temperature profile of the fluid $k_BT$ calculated using the equipartition theorem as a function of $x$. The thermostat maintains the desired uniform temperature $k_BT = 1$ of the flowing fluid.

those particles which exit the box at $x = 0$ and at $x = L_x$ are put back into the system, as explained in the previous sections. The idea of redistributing particles along the length of the box with a uniform probability is akin to the experimental realization suggested in Fig. 2 but with infinite number of entry points in the tube. Our model of the idealized uniaxial exponential-stretched flow can nearly be obtained at the axis of symmetry of a four-roll geometry producing extensional flow or at the centerline of flow in a filament-stretching rheometer.

To make our measurements more quantitative, we plot the the linearly increasing velocity profiles of the MPC fluid as a function of $x$ for different values of the flow rate $\epsilon$ with $v_0 = 0$ in Fig. 4(a). We get consistent velocity profiles of the fluid in tune with our expectations for all values of $\epsilon$ except for $\epsilon = 0.002/\tau$. The flow with the highest value of $\epsilon$ shows deviations from the linear profile; but in this case the maximum velocity of the fluid at $x = L_x$ reaches $0.05c_s$ and the method is expected to start showing artifacts. The slope of the velocity profiles gives the actual velocity gradient $\epsilon^*$ as obtained from our simulations.

To compare it to the value of applied velocity gradient $\epsilon$ in the expression for $f_E^x$ in Eq. (2), we plot $\epsilon^*/\epsilon$ for the different values of $\epsilon$ used to obtain the ES flows. This is shown in Fig. 3(b). The values of the ratio $\epsilon^*/\epsilon$ are very close to 1 which is a very satisfactory validation of the required flow. The value of $\epsilon^*/\epsilon$ for only the largest value of $\epsilon = 0.002\tau^{-1}$

shows around 3% deviation from the perfect value of 1, but this is again the case where the velocity at $x = L_x$ becomes $0.08a/\tau$ (i.e., about 5% of $c_s$, the sound velocity). This is the case which shows a clear deviation from the linear velocity profile [refer to Fig. 4(a)]. Thus, unless one uses $v_x^{\max} \ll c_s$, the method is expected to fail for reasons mentioned before. Thus we also investigate the regime where the validity of the scheme starts becoming suspect; clearly in all future simulations one should use ES flow rates $\epsilon$ which lead to fluid velocities $v_x^{\max} < 0.04a/\tau$ at the $x = L_x$ end.

Figures 4(c) and 4(d) show the number density $\rho(x)$ and temperature $k_BT$ of the fluid particles along the length of the channel for two different box sizes. The density has been normalized by the average number density $\rho_0$, which is 10 particles per $a^3$, the volume of each collision box. For all values of $\epsilon < 0.001\tau^{-1}$ (such that at $x = L_x = 40a$, the maximum fluid velocity $v_x^{\max} < 0.03c_s$ is maintained) the deviation from the average density is $\sim$1%. The figure establishes that the density of the fluid $\rho(x)$ is held constant along the length of the channel and our idea of introduction of $\langle N_\epsilon \rangle$ MPC particles after every ballistic step, at random positions between $x = 0$ and $x = L_x$, is a reasonable one. For the smaller box size of $(20a)^3$, the deviation in the density is $\sim$1% even if $\epsilon = 0.001\tau^{-1}$ or $0.002\tau^{-1}$ is used. This is because the maximum velocity at $x = L_x$ for the smaller box with $L = 20a$ is half the value of $v_x^{\max}$ for the box of size $(40a)^3$. The thermostat maintains the temperature of the fluid at the desired value with less than 1% deviation at even higher values of $\epsilon$ used in the simulation. Of course, for both $\rho$ and $k_BT$ there are edge effects at $x = 0 = L_x$, but for the low $\epsilon$ values that we use in future simulations, the effects are minimal.

One also sees a mild density gradient along the length of the channel although this is negligible at low values of $\epsilon$. We think the applied flow perturbs the Maxwell-Boltzmann velocity distribution, especially at the $x = L_x$ end, although we apply a local thermostat every 50 iterations to maintain the right temperature. This in turn perturbs the theoretical calculation of the number of particles to be from moved from the left end of the box to the right and vice versa, as well as the number of particles being redistributed in the box. Thus for lower values of $\epsilon$, such that the maximum velocity at the right end of the box is low, one sees a lower density gradient. Even for the largest $\epsilon = 0.002\tau$ used in the simulation, one sees a large density gradient for a $40 \times 40 \times 40a^3$ box but a reduced density gradient for a smaller $20 \times 20 \times 20a^3$ box.

A viable apprehension is that hydrodynamic interactions between suspended particles might be destroyed by the addition of fluid particles at random positions in the simulation box. With that consideration we calculate the fraction of reintroduced particles $N_\epsilon(T)$ in time $T$ in a box of length $L_x \times L_y \times L_z$, where $T$ is the time taken for diffusion of momentum of the fluid over half the length of the simulation box. We choose $L_x = L_y = L_z = 40a$ and the number density $\rho = 10/a^3$, and then the kinematic viscosity $\nu = \eta/m\rho \approx 0.83a^2\tau^{-1}$ for the values of rotation angle $\alpha$ and collision time $h$ chosen for this simulation (refer to [36,40] for calculation of the viscosity $\eta$). Thereby $T = (20a)^2/(6\nu) \approx 80\tau$. The average number of particles exiting the $x = L_x$ surface in time $\tau$ due to flow is $(\epsilon L_x)\rho(L_yL_x) = 640$ particles for $\epsilon = 0.001\tau^{-1}$. These particles are put back at random positions in the box with 640 000 MPC partcles, and thereby 8% of the particles are replaced at random positions in time $T = 80\tau$. This gives the upper limit of the number of fluid particles introduced at random positions as typically lower values of $\epsilon$ will be used in a similar-sized box. We also show later that the velocity autocorrelation function of a suspended macromolecule in the MPC fluid undergoing ES flow decays as a power law, which is one of the signatures of having incorporated hydrodynamics in describing the dynamics of a particle in a fluid.

## III. MACROMOLECULES IN ES FLOW

The interest of the soft matter and rheology community lies, of course, in studying the response of colloids, polymers, and macromolecules in steady-state uniaxial elongational flows or the nearly equivalent ES flow. To that end, we study the response of two test cases, a suspension of colloids with only excluded volume (EV) interactions between them in the nearly equivalent exponential-stretching flow and also an extended object with internal degrees of freedom such as a polymer in ES flow. In particular we have done simulations with a star polymer with different numbers of arms $f$ in ES flow. In the following, the issue of PBCs of these macromolecules embedded in the MPC fluid is addressed over and above modeling ES flow of the background MPC fluid.

### A. Colloids in ES flow

We introduce 2000 spherical colloids coupled to the MPC fluid in a $(500 \times 10 \times 10)a^3$ box filled with $1 \times 10^6$ MPC fluid particles (number density $\rho_{fl} = 20$) and apply a position-dependent force $f_E^x$, as defined in Eq. (2), to both colloidal and MPC particles. We use $\epsilon = 0.000\,05\tau^{-1}$ such that the maximum velocity $v_{\max}$ is $0.025a/\tau$ at the $x = L_x = 500a$ end, which ensures that $v_{\max} < 0.02c_s$. The colloids interact with each other via the Lennard-Jones potential

$$V_{LJ} = 4\epsilon_c\left(\frac{\sigma_c^{12}}{r^{12}} - \frac{\sigma_c^6}{r^6}\right) \tag{4}$$

suitably shifted and truncated at $r_{\text{cut}} = 2^{1/6}\sigma_c$ such that there exists only repulsive excluded volume interactions between the colloids. We have used the colloidal radius $r_c = \sigma_c/2 = 0.4a$, $\epsilon_c/k_BT = 1$, and colloidal mass $m_c = 20m_f$ such that the colloids are density matched with the background MPC fluid. The position and velocity of the colloids are updated every $t_{\text{MD}} = 0.0025\tau$; this is the time step for MD simulations. The momentum-exchanging rotation step of colloids + MPC fluid particles is implemented after every 40 MD steps, such that $h$ remains $0.1\tau$, where $\tau$ is defined as before as $\tau = \sqrt{m_f a^2/k_BT}$.

The colloids are coupled to the MPC fluid and exchange momentum with it; this is achieved by including the embedded colloid in the rotation step of the MPC dynamics where momentum is redistributed among the fluid particles. There is EV interaction between the colloidal spheres, but with respect to the MPC fluid the colloids are just pointlike particles with a mass of $20m_f$. The details of this coupling scheme between an embedded particle and the MPC fluid and the success of the scheme are well explained in Refs. [36,40]. PBCs for the

colloids in ES flow are implemented thus: We put back all colloids which cross the $x = L_x$ (alternatively $x = 0$) boundary into the box at $x = 0$ $(x = L_x)$ with the $x$ component of the colloid velocity $v_x^c$ suitably reduced (increased) by $\epsilon L_x$.

We start our simulation with 2000 model colloid particles arranged in a cubic lattice in the simulation box. We switch on ES flow as described above and allow $0.4 \times 10^6$ iterations ($0.4 \times 10^6$ MPC particle position and velocity updates, or $16 \times 10^6 t_{\rm MD}$) for the system to reach steady state. We then start calculating the number distribution of colloids as a function of flow direction $x$ in the steady state over the next $0.8 \times 10^6$ iterations. At steady state, a fixed number of colloid particles enters the simulation box by crossing the $x = 0$ plane per unit time, and the same number exits via the $x = L_x$ plane. The lower number density of colloids at the $x = L_x$ end is offset by the larger velocities of the particles in the flow direction, thereby maintaining uniform current density. For comparison we have also studied the case where there are 3000 colloid particles in the $500a \times 10a \times 10a$ box. We choose the velocity of colloids at the $x = 0$ plane to be $v_0 = 0.01a/\tau$ to minimize aggregation of particles at that boundary.

Figure 5 (top) shows a snapshot of 2000 colloids particles in steady-state ES flow. There is a distinct decrease in the number density of colloids with increasing $x$; near $x = 0$ there is a very high density of particles extended to about $x = 100a$. If $\vec{J}_c(x) = n(x)\vec{v}_c(x)$ is the colloidal current density in ES flow, $\vec{\nabla} \cdot \vec{J}_c = 0$ implies $n(x) \sim 1/x$ where $n(x)$ is the number density of colloids and $\vec{v}_c(x) = \epsilon x + v_0$ is their velocity in ES flow. The middle and bottom figures show snapshots of the 3000 colloids after $0.4 \times 10^6$ and $0.6 \times 10^6$ iterations, respectively. The system clearly has not reached steady state; furthermore, it seems that the region with high density of colloids shows behavior reminiscent of *jamming* and is moving together as a block in the ES flow. This is in tune with experimental studies which also see jamming

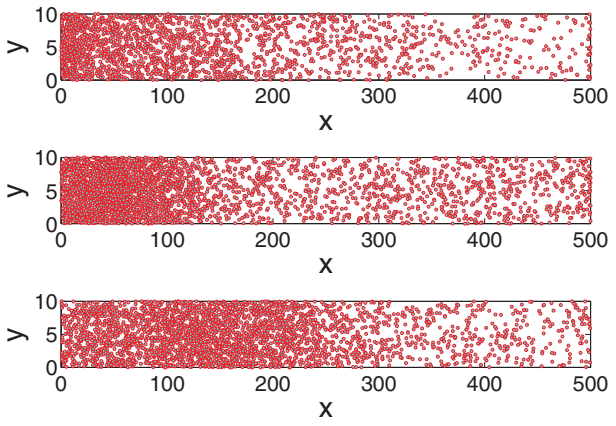


FIG. 5. (Color online) Snapshot of 2000 (top figure) colloidal particles with excluded volume interactions in steady-state ES flow in the $x$ direction with the background fluid modeled by MPC dynamics. The velocity gradient is $\epsilon = 0.000\,05\tau^{-1}$ with box dimensions $L_x = 500a$ and $L_y = L_z = 10a$. The bottom two figures show 3000 particles in the flow at two different time instants. The bottom figure suggests a local jamming of colloids at $x = 150a$ where the particles in the high-density region move cooperatively in the positive $x$ direction.

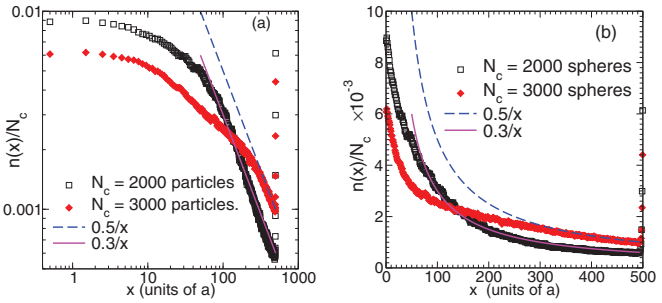


FIG. 6. (Color online) Number of particles $n(x)$, normalized by the total number of particles $N$, as a function of $x$ undergoing ES flow for $N = 2000$ and $N = 3000$ in a $500a \times 10a \times 10a$ box plotted on a log-log scale. The continuous lines ($0.5/x$ and $0.3/x$) have been plotted to aid the reader to compare with the expected $1/x$ dependence of the number density of colloidal particles in ES flow. The data shown in (b) are the same as those shown in (a) but plotted on a linear scale.

of colloidal suspensions in extensional flow [49]. However, a detailed investigation and understanding of the observed phenomenon is an ongoing project and will be reported in a future communication.

We focus on the $N = 2000$ colloids case and show the number density of colloids $n(x)$ as a function of $x$ in a linear plot as well as in a log-log plot in Fig. 6. The density shows a $1/x$ dependence for $x > 100a$ as expected on solving the continuity equation with $\partial\rho/\partial t = 0$. We have also plotted the function $0.5/x$ which lies exactly on $n(x)$ to illustrate that the density indeed falls as $1/x$ along the length of the channel. We have also shown $n(x)$ versus $x$ for $N = 3000$ particles, albeit its has not reached steady state and there could be other physics at play as discussed above.

We can envisage the region $0a < x < 500a$ to be a fluid-filled tube in the laboratory with the appropriate velocity profile in which particles enter at $x = 0$ and leave at $x = 500a$, so that there are boundary effects at $x = 0$ and $x = L_x$. However, in the region $100a < x < 500a$ we have steady-state exponential-stretching flow, and this region can be used to calculate statistical properties of interacting colloids in ES flow.

### B. A star polymer in ES flow

The modeling of extended objects like polymers is more complicated than the flow of colloidal particles, which have been considered as pointlike objects with respect to the fluid. The fundamental problem in applying PBCs for extended objects is that, as one end of the object (say a few monomers in the front) crosses the $x = L_x$ boundary, they cannot be put back in the box at the $x = 0$ end with a suitably reduced value of $v_x$ of the colloid. This is because the polymer is spread on either side of the $x = L_x = 0$ plane and there the velocity gradient becomes $\infty$. This in turn will affect the steady-state structural properties of the polymer. Thus when invoking PBCs for the polymer or macromolecule, the entire polymer has to be shifted to the other end of the box such that the polymer remains in a uniform velocity gradient. Before we discuss in greater detail how we implement PBCs for extended polymeric objects, we briefly describe our bead-spring polymer model and its coupling with the fluid.

We consider a star polymer in a simulation box $(L_x \times L_y \times L_z)a^3$ with the PBCs for fluid in ES flow as described earlier. Each monomer of the polymer is acted upon by a force depending upon its position as in Eq. (2). The coupling between monomer and the MPC fluid is achieved in the collision step and each monomer is a point particle just like the other fluid particles but with a mass $10m_f$, as $\rho_f = 10$ for these simulations. There is no other interaction (EV or otherwise) between the monomers and the fluid particles. A linear polymer is just a star with two arms. The number of monomers in each arm is $N_p = 30$ and the length of each arm is $L_p = N_p r_p$, where $r_p$ is the length of the bond between adjacent monomers. We chose $r_p = a = 1$; the interaction between neighboring monomers in a chain separated by distance $r$ is $V(r) = \kappa(r - r_p)^2$, with $\kappa = 1000k_BT$, so that we have nearly inextensible bonds in our bead-spring model of polymers. In addition, to model good solvent conditions we implement an excluded volume interaction between monomers by a Lennard-Jones potential between monomers with $\sigma_p = 0.8a$, where $\sigma_p$ is the diameter of a monomer. The potential is suitably truncated at $r = 2^{1/6}\sigma_p$ and shifted so that we have only repulsive interactions between the monomers. The polymer arms emanate out from a central monomer, the center-to-center distance and bond length between the central monomer and the first monomer in different arms being $\sigma_p^c = 2.0a$ and $r_p^c = 2.0a$, respectively.

The crucial idea in the implementation of PBCs of a star polymer (or some other macromolecule) is this: We restrict the center of the polymer to move between $x_L = \ell$ and $x_R = L_x - \ell$ ($\ell \leqslant L_x/2$), but implement the usual PBCs in the $y$ and $z$ directions. As soon as the central monomer crosses $x_R$ in ES flow, the central monomer (and all monomers) are shifted to position $x_L$ (at appropriate positions relative to $x_L$) with an accompanying velocity shift of $\epsilon(L_x - 2\ell)$ for the $x$ component of the velocity of each monomer. Note than in this case, the polymer always experiences a uniform velocity gradient as long as $L_x > 2\ell$.

Moving the entire polymer from near the $x = L_x$ end to the $x = 0$ end of the simulation box maintains the velocity gradient across the polymer, but the fluid around the star needs to be moved as well, along with the star, to maintain correct streamlines, hydrodynamics, and PBCs. To this end, we move all the fluid particles contained between $(L_x - 2\ell)$ and $L_x$ to the volume between $0 < x < 2\ell$ at the same time that PBCs are invoked for the monomers of the polymer. Correspondingly the fluid between $0 < x < (L_x - 2\ell)$ is displaced in the positive $x$ direction by distance $2\ell$. There must be corresponding velocity shifts of $-\epsilon(L_x - 2\ell)$ and $+2\epsilon\ell$, respectively, in the velocity of the shifted particles. Thus one can implement the PBCs of the polymer-fluid system without changing the fluid flow around the polymer. The relative positions of the fluid particles also remain unchanged with respect to each other. A schematic figure is given in Fig. 7 for ease of visualization by the reader.

We use a simulation box of dimensions $(100 \times 40 \times 40)a^3$ for star polymers with $f = 2$, 5, and 10 arms and a box of size $(120 \times 40 \times 40)a^3$ when $f = 20$. There are $1.6 \times 10^6$ MPC fluid particles in the box of length $100a$ and $1.92 \times 10^6$ fluid particles for $L_x = 120a$ such that $\rho_{fl} = 10a^{-3}$ always. The quantity $\ell$ was chosen to be $25a$ and $30a$ for $L_x = 100a$ and $L_x = 120a$ (for $f = 20$), respectively. The mass of each

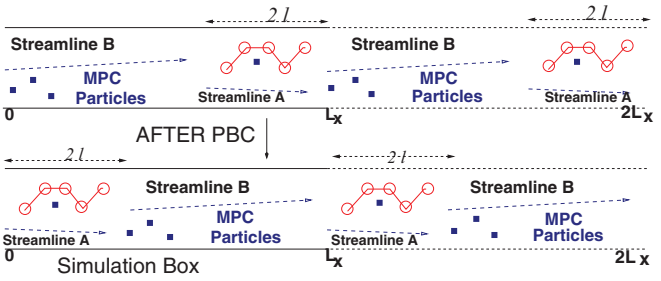


FIG. 7. (Color online) Schematic diagram describing the method we use to implement PBCs for polymers in ES flow. The MPC fluid is contained between $L_x - 2\ell$ and $L_x$ surrounding a polymer, and the polymer itself is shifted to the left end of the box from the right end when the center of the polymer crosses position $x = L_x - \ell$. A suitable velocity shift is applied along with change in the position. The quantity $\ell$ is chosen such that the length of the polymer in the stretched condition $(N_p r_p)$ should $\leqslant 2\ell$. Simultaneously the fluid contained to the left of $L_x - 2\ell$ is moved to the right by an amount $2l$ with the appropriate velocity shift. The box with dashed lines shown between $L_x$ and $2L_x$ represents a periodic image of the actual simulation box between 0 and $L_x$.

monomer $m_p = 10m_f$ such that each monomer was again density matched with the fluid. The time step for MD is $t_{\rm MD} = 0.005\tau$, and the MPC rotation and position update is carried out every 20 MD steps, such that $h = 0.1\tau$. We allowed $0.1 \times 10^6$ MPC iterations for the system to reach steady state, data for thermodynamic averages were collected over the next $0.35 \times 10^6$ MPC iterations, and structural quantities were averaged over at least seven independent runs.

The top and middle pictures in Fig. 8 show snapshots of polymer configurations of a star with $f = 2$ (equivalent to a linear polymer chain of length $2N_p + 1$, by including the central monomer in the count) at two different flow rates. The bottom picture is a snapshot of two different configurations of a star with $f = 20$ at the higher flow rate. We clarify that we simulate only one star in the flow; the stars shown in different colors are snapshots of the same single star at different time instants as it moves along the flow. Note that as soon as the $f = 2$ star crosses $x = 75a$ ($\ell = 25a$) to the right, the entire star is shifted to $x = 25a$. Simultaneously, the fluid particles with $x$ coordinates in the range $50a < x < 100a$ are shifted to the region $0 < x \leqslant 50a$, and the particles which occupy the region $0 < x \leqslant 50a$ are shifted to the right by $2\ell$ and now fill the region $50a < x < 100a$. Thus the relative positions of the fluid particles remains unchanged with respect to each other in this implementation of PBCs. Of course, the appropriate velocity shift has to accompany the position shift. For the $L_x = 120a$ box (bottom picture), $\ell = 30a$, and as soon as the star center crosses $x = 90a$, all the particles in the region $60a < x < 120a$ are shifted to $0 < x < 60a$ and vice versa.

We use $\tau_R = \eta_S r_p^3 N_p^2/k_BT = \tau_0 N_p^2$ to calculate the relaxation time $\tau_R$ of a polymer arm of length $N_p r_p$ and bond length $r_p$, where $\eta_S$ is the solvent viscosity and $\tau_0 = \eta_S r_p^3/k_BT$ [50,51]. We would like to clarify that the Zimm model for an ideal polymer chain (i.e., in $\theta$ solvent) predicts the length dependence of the relaxation time to be $\tau_\theta^Z \sim N_p^{3\nu} \sim N_p^{1.5}$ for $\nu = 0.5$. But for polymers in good solvents with EV interactions among polymer chains (as is the case in our

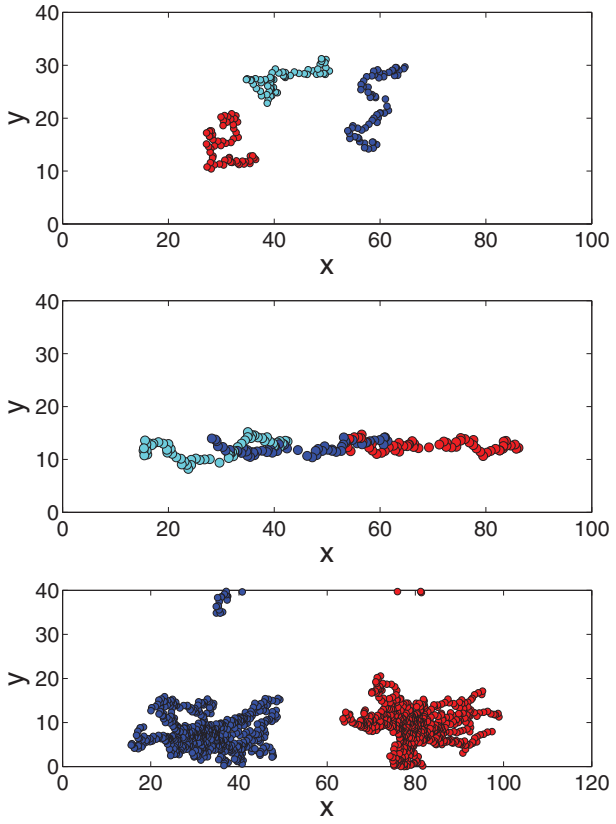


FIG. 8. (Color online) The top and middle figures show the polymer configurations of a linear polymer chain (star polymer with $f = 2$ and $N_p = 30$ monomers in each arm) in ES flow with Weissenberg numbers $\mathrm{Wi} = \epsilon\tau_R = 0.324$ and $\mathrm{Wi} = 1.944$, respectively. $\tau_R$ is the relaxation time of a star-polymer arm. The three-polymer configurations shown with different shades (colors) represent the same polymer but at different simulation times and thereby at different positions in space. The bottom figure shows a star with $f = 20$ in ES flow with $\mathrm{Wi} = 1.944$. As before the two differently shaded (colored) stars refer to configurations of the same polymer at two different simulation times. The polymers are stretched for $\mathrm{Wi} > 1$.

simulations), the Zimm prediction for relaxation times is $\tau^Z_{EV} \sim N_p^{3\nu} \sim N_p^{1.8}$ for $\nu = 0.6$, $\nu$ is the scaling exponent which describes the variation of the size of the polymer with the length of the polymer chain. However, for different simulations of polymers in good solvents one observes the relaxation time dependence of polymer chains with the number of monomers in a chain as $\sim N_p^2$ [50–52], and therefore we use $\tau_R \sim N_p^2$ as an estimate of the relaxation time of the star, as has been done previously in the literature. In our simulations with $N_p = 30$ monomers, $\tau_R = 900\tau_0$ and $\tau^Z_{EV} = 456\tau_0$ such that $\tau_R \approx 2\tau^Z_{EV}$.

One can unambiguously see in Fig. 8 that the polymers get stretched for Weissenberg number $\mathrm{Wi} = \epsilon\tau_R > 1$. The stretching of stars is explored systematically in Fig. 9 where we plot the diagonal components $G_{\alpha\alpha}$ of the gyration tensor $G_{xy}$ at different flow rates, normalized by the average of the diagonal components of the gyration tensor $G_0$ when $\epsilon = 0$, where $\alpha = x$, $y$, or $z$. The quantity $G_{\alpha\alpha}$ for $\alpha = x$ is defined

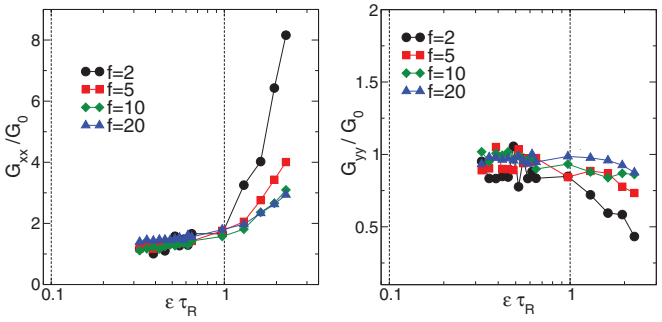


FIG. 9. (Color online) Diagonal components of the gyration tensor $G_{xx}$ and $G_{yy}$ plotted versus the Weissenberg number $\mathrm{Wi} = \epsilon\tau_R$ for different numbers of arms $f$, in order to study the structural response of the star to ES flow. The fluid flows in the $x$ direction. $G_{xx}$ and $G_{yy}$ have been normalized by $G_0$, the average of the diagonal components of the gyration tensor in equilibrium (i.e., no flow). The vertical lines at $\epsilon_c\tau_R = 1$ and $\epsilon\tau_R = 0.1$ are to aid the eye.

as

$$G_{xx} = \frac{1}{2N_p + 1}\sum_i (x_i - x_{cm})(x_i - x_{c.m.}), \tag{5}$$

where $x_{c.m.}$ is the $x$ coordinate of the center of mass of the star. In Fig. 9 we show the variation of $G_{xx}$ and $G_{yy}$ as a function of $\mathrm{Wi} = \epsilon\tau_R$ for a star with different numbers of arms in ES flow. There is a sharp transition beyond a critical $\mathrm{Wi}_c = 1$, where the stars get extended. This is in tune with experimental observations of flexible polymers in E flow [53,54]. For $\mathrm{Wi} < 1$, we observe linear response of the star to the ES flow, where $G_{xx}$ increases linearly with $\epsilon$, but the response becomes nonlinear above $\mathrm{Wi} \approx 1$ for all values of $f$. Correspondingly, there is a reduction in size of the star in directions perpendicular to the flow, i.e., the $y$ and $z$ directions. Interestingly, the critical $\mathrm{Wi}_c$ does not seem to depend significantly on the number of arms; at least up to $f = 20$, its polymeric behavior is retained.

We clarify this because a star polymer is a very interesting soft matter system, in which by just tuning the number of arms of a star one can possibly go from a rigid colloidlike object to a polymeric macromolecular system. A star with many arms has a very dense rigid core and is not easily deformable, i.e., it is almost colloidlike. On the other hand, a star with $f = 2$ is just a linear polymer chain. We further point out that we could calculate the Weissenberg number as $\mathrm{Wi}^Z = \epsilon\tau^Z_{EV} = \epsilon\tau_R/2$ and use this to investigate the variation of $G_{\alpha\alpha}$ with $\epsilon$. But the only difference will be that $\mathrm{Wi}^Z \approx 1$ will be obtained at double the presently used value of $\epsilon_c$, and the vertical lines in Fig. 9 will shift to the right. The critical value $\epsilon_c$ is the flow rate at which $\mathrm{Wi} = 1$.

To convince ourselves and the reader that hydrodynamics is correctly incorporated in spite of (i) the reintroduction of MPC particles which are exiting the simulation box in the $+\hat{x}$ direction and (ii) the repositioning of the macromolecule + fluid from the right end of the box (near $x = L_x$) to the left end of the box (near $x = 0$) for implementation of PBCs, we have computed the time relaxation of the velocity-velocity autocorrelation function (VCF) for the center of mass of a star polymer with $f = 20$. We show the plot of VCF versus time,

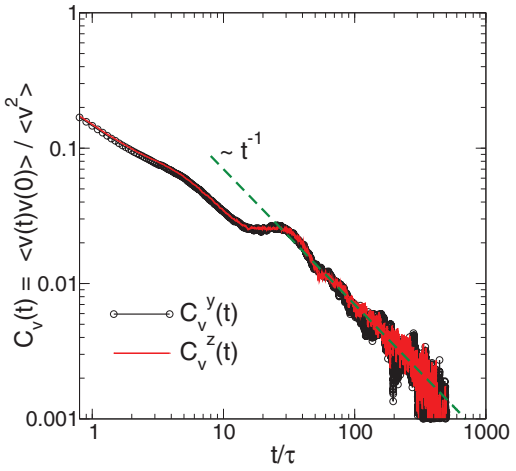


FIG. 10. (Color online) Velocity correlation functions $\langle v(t)v(0)\rangle$ versus time $t$ in the $y$ and $z$ directions, i.e., directions perpendicular to the flow direction, of the center of mass (c.m.) of a star polymer with $f = 20$ arms, suspended in a MPC fluid undergoing ES flow with $\epsilon = 0.0002\tau^{-1} \equiv \mathrm{Wi} = \epsilon\tau_R = 1.3$. For $t > 30\tau$, the VCF shows a $t^{-1}$ decay of VCF with time. The dashed green line is to aid the reader to estimate the exponent of the power-law decay of the computed VCFs. The VCFs have been normalized by the average of the square velocity of the c.m. of the star, and time is measured in units of $\tau^2 = m_f a^2/k_B T$.

suitably normalized, in Fig. 10. Data shown are averaged over 80 independent runs with $\epsilon = 0.0002\tau^{-1} \equiv \mathrm{Wi} = \epsilon\tau_R = 1.3$, where $\tau_R$ is the relaxation time of the polymer. At long times when the hydrodynamics is developed and momentum transport by background fluid should affect the diffusive behavior of the star, particularly in the $y$ and $z$ directions perpendicular to the flow direction, our simulations show that the VCF decays nearly as $\sim t^{-1}$ for $t > 30\tau$. We try to understand this by observing that momentum conservation is maintained only in the two directions transverse to the flow. Absence of hydrodynamics would have resulted in the exponential decay of the VCF. From this we conclude that hydrodynamic effects due to momentum conservation between the star and background fluid are maintained even at relatively high ES flow gradients. At times below $t = 30\tau$, i.e., before diffusive time scales are reached, we see the average effect of relaxation of many polymer arms on the center of the star. We need to investigate further to understand the presence of the knee in the VCF just before $t < 30\tau$.

## IV. DISCUSSION

We have introduced a method to obtain exponentially stretching flow, a slight variant of steady-state uniaxial extensional flow of a fluid, by computer simulations. Just as the velocity field in uniaxial flow extensional flow, ES flow has the velocity field $v_x = \epsilon x$ in the flow direction. We also study the response of two simple test systems, viz., a colloidal system with only excluded volume interactions and a linear polymeric system in ES flow. We extend our study to star polymers in ES flow. Since the response of macromolecules in ES flow is the same as that in extensional flow, we suggest that this will be a reliable method to study the response of soft matter systems in *steady-state* E flow, which is difficult to obtain experimentally and in simulations.

For a coarse-grained MPC fluid undergoing ES flow under steady-state conditions, we have obtained a linearly increasing velocity profile in the direction of flow in tune with our expectations. We also maintain the density of fluid constant along the length of the flow by suitable reintroduction of MPC fluid particles along the length of the channel of uniform cross section. We have demonstrated that the temperature of the fluid is held constant along the length of the flow by using a suitable thermostat. The measured flow velocity gradient $\epsilon^*$ is equal to the applied velocity gradient $\epsilon^*$ as long as the maximum velocity of the fluid is significantly less than the sound velocity of the fluid. Care must be taken that the calculated value of $\langle N_\epsilon\rangle$, the number of particles to be redistributed at random positions in the box, is an integer number. This can be achieved by suitably choosing the value of $\epsilon$ or $L_x, L_y, L_z$ in the expression for calculating $\langle N_\epsilon\rangle$. The total number of particles (mass of fluid) in the simulation box is always exactly conserved globally, as only the excess fluid flowing out of the right end of the simulation box is put back along the length of the box to maintain fixed density along the flow direction. We have also established that the slow and gradual reintroduction of fluid particles in the flow channel does not destroy hydrodynamic correlations built up due to momentum conservation between a diffusing particle and the fluid around it.

The response of dilute systems of simple macromolecules (colloids and polymers) dispersed in a fluid undergoing ES flow is also in tune with previous studies by other groups on similar systems in E flow. This gives us further confidence that we are correctly modeling ES flow despite the apparently unphysical introduction of MPC particles at random positions within the simulation box. We thus think that the method can be used to study a wide range of soft matter systems. We are not aware of any previous studies of the response of star polymers to E flow or ES flow, though the response of linear polymers to E flow is well reported in the literature. We see in our simulations that star polymers undergo a coil-stretch transition when $\mathrm{Wi}_c = \epsilon\tau_R > 1$, where $\tau_R$ is the relaxation time of a polymer equal in length to that of a star-polymer arm. We do not observe any dependence of this critical Weissenberg number on the number of arms $f$ of the star. Any sensitive dependence, if it exists, is not discernible from the available data.

The modeling of multiple extended objects (many polymers) in ES flow under steady-state conditions is an ongoing work and will be reported in a future communication.

## ACKNOWLEDGMENTS

A.C. acknowledges the use of the computer cluster available for the Nano-Science unit in IISER, which is funded by DST, India by Project No. SR/NM/NS-42/2009. A.C. further acknowledges very useful discussions with K. Guruswamy and Arijit Bhattacharyay during the course of this work.

[1] G. H. McKinley and T. Sridhar, Annu. Rev. Fluid Mech. **34**, 375 (2002).
[2] S. L. Anna, G. H. McKinley, D. A. Nguyen, T. Sridhar, S. J. Muller *et al*., J. Rheol. **45**, 83 (2001).
[3] P. Doyle, E. S. G. Shaqfeh, G. H. McKinley, and S. H. Spiegelberg, J. Non-Newtonian Fluid Mech. **76**, 79 (1998).
[4] V. Tirtaatmadja and T. Sridhar, J. Rheol. **37**, 1081 (1993).
[5] V. Tirtaatmadja and T. Sridhar, J. Rheol. **39**, 1133 (1995).
[6] T. Sridhar, J. Non-Newtonian Fluid Mech. **35**, 85 (1990).
[7] C. J. S. Petrie, J. Non-Newtonian Fluid Mech. **137**, 1 (2006).
[8] C. J. S. Petrie, J. Non-Newtonian Fluid Mech. **137**, 15 (2006).
[9] Y. Rabin, J. Non-Newtonian Fluid Mech. **30**, 119 (1988).
[10] H. A. Barnes, J. F. Hutton, and K. Walters, *An Introduction to Rheology* (Elsevier, Amsterdam, 1989).
[11] A. M. Kraynik and D. A. Reinelt, Int. J. Multiphase Flow **18**, 1045 (1992).
[12] J. M. Kim, D. J. Keffer, M. Kroeger, and B. J. Edwards, J. Non-Newtonian Fluid Mech. **152**, 168 (2008).
[13] M. Kroeger, C. Luap, and R. Mueller, Macromolecules **30**, 526 (1997).
[14] J. Fang, M. Kroeger, and H. C. Oettinger, J. Rheol. **44**, 1293 (2000).
[15] M. L. Matin, P. J. Davis, and B. D. Todd, J. Chem. Phys. **113**, 9122 (2000).
[16] B. D. Todd and P. J. Daivis, Phys. Rev. Lett. **81**, 1118 (1998).
[17] B. D. Todd and P. J. Daivis, Comput. Phys. Commun. **117**, 191 (1999).
[18] B. D. Todd and P. J. Daivis, J. Chem. Phys. **107**, 1617 (1997).
[19] I. M. Neelov, D. B. Adolf, A. V. Lyulin, and G. R. Davies, J. Chem. Phys. **117**, 4030 (2002).
[20] T. T. Perkins, D. E. Smith, and S. Chu, Science **276**, 2016 (1997).
[21] D. E. Smith and S. Chu, Science **281**, 1335 (1998).
[22] R. G. Larson, H. Hu, D. E. Smith, and S. Chu, J. Rheol. **43**, 267 (1999).
[23] C. M. Schroeder, H. P. Bobcock, E. S. G. Shaqfeh, and S. Chu, Science **301**, 1515 (2003).
[24] C. M. Schroeder, E. S. G. Shaqfeh, and S. Chu, Macromolecules **37**, 9242 (2004).
[25] E. S. G. Shaqfeh, J. Non-Newtonian Fluid Mech. **130**, 1 (2005).
[26] B. D. Hoffman and E. S. G. Shaqfeh, J. Rheol. **51**, 947 (2007).
[27] I. Dukovski and M. Muthukumar, J. Chem. Phys. **118**, 6648 (2003).
[28] S. Liu, B. Ashok, and M. Muthukumar, Polymer **45**, 1383 (2004).
[29] T. A. Hunt and B. D. Todd, J. Chem. Phys. **131**, 054905 (2009).
[30] T. A. Hunt, S. Bernardi, and B. D. Todd, J. Chem. Phys. **133**, 154116 (2010).
[31] S. Somani, E. S. G. Shaqfeh, and J. Ravi Prakash, Macromolecules **43**, 10679 (2010).
[32] D. Petera and M. Muthukumar, J. Chem. Phys. **111**, 7614 (1999).
[33] P. Sunthar and J. Ravi Prakash, Macromolecules **38**, 617 (2005).
[34] A. Malevanets and R. Kapral, J. Chem. Phys. **110**, 8605 (1999); **112**, 7260 (2000).
[35] R. Kapral, Adv. Chem. Phys. **140**, 89 (2008).
[36] M. Ripoll, K. Mussawisade, R. G. Winkler, and G. Gompper, Phys. Rev. E **72**, 016701 (2005); K. Mussawiade, M. Ripoll, R. G. Winkler, and G. Gompper, J. Chem. Phys. **123**, 144905 (2005).
[37] E. Allahyarov and G. Gompper, Phys. Rev. E **66**, 036702 (2002); M. Ripoll, K. Mussawiade, R. G. Winkler, and G. Gompper, Europhys. Lett. **68**, 106 (2004).
[38] N. Kikuchi, C. M. Pooley, J. F. Ryder, and J. M. Yeomans, J. Chem. Phys. **119**, 6388 (2003).
[39] C. M. Pooley and J. M. Yeomans, J. Phys. Chem. B **109**, 6505 (2005).
[40] G. Gompper, T. Ihle, D. M. Kroll, and R. G. Winkler, Adv. Polym. Sci. **221**, 1 (2009).
[41] I. O. Götze, H. Noguchi, and G. Gompper, Phys. Rev. E **76**, 046705 (2007).
[42] J. T. Padding and A. A. Louis, Phys. Rev. Lett. **93**, 220601 (2004).
[43] J. T. Padding and A. A. Louis, Phys. Rev. E **74**, 031402 (2006).
[44] J. T. Padding and A. A. Louis, Phys. Rev. E **77**, 011402 (2008).
[45] T. Ihle and D. M. Kroll, Phys. Rev. E **67**, 066705 (2003); **67**, 066706 (2003).
[46] E. Tüzel, M. Strauss, T. Ihle, and D. M. Kroll, Phys. Rev. E **68**, 036701 (2003); T. Ihle, E. Tüzel, and D. M. Kroll, *ibid*. **70**, 035701(R) (2004); **72**, 046707 (2005).
[47] B. Duenweg and A. J. C. Ladd, Adv. Polym. Sci. **221**, 89 (2009).
[48] C. C. Huang, A. Chatterji, G. Sutmann, G. Gompper, and R. G. Winkler, J. Comput. Phys. **229**, 168 (2010).
[49] M. I. Smith, R. Besseling, M. E. Cates, and V. Bertola, Nat. Commun. **1**, 114 (2010).
[50] M. Ripoll, R. G. Winkler, and G. Gompper, Phys. Rev. Lett. **96**, 188302 (2006).
[51] M. Ripoll, R. G. Winkler, and G. Gompper, Eur. Phys. J. E **23**, 349 (2007).
[52] C. Aust, M. Kröger, and S. Hess, Macromolecules **32**, 5660 (1999).
[53] A. Keller and J. A. Odell, Colloid Polym. Sci. **263**, 181 (1985).
[54] L. Xue, U. S. Agarwal, and P. J. Lemstra, Macromolecules **38**, 8825 (2005).